Journal of Fluids and Structures (2002) **16**(3), 375–390
doi:10.1006/jfls.2001.0424, available online at http://www.idealibrary.com on IDEAL®

DYNAMIC SIMULATION OF MARINE RISERS MOVING RELATIVE TO EACH OTHER DUE TO VORTEX AND WAKE EFFECTS

S. I. Sagatun and K. Herfjord

Norsk Hydro ASA-Exploration and Production Bergen, Norway

and

T. Holmås

SINTEF MT Structural Engineering Trondheim, Norway

(Received 8 July 1999, and in final form 21 September 2001)

This article presents a time domain simulator which simulates the dynamic interaction of two adjacent cylindrical risers moving relative to each other in an ambient steady flow. The main objective of the simulator is to assess whether adjacent marine risers moving in each other's wake will collide or not. The simulator named Time domain RIser Collision Evaluation (TRICE) uses drag and lift coefficients as well as excitation frequencies computed by an in-house developed numerical Navier–Stokes equation solver (CFD). The CFD program computes lift and drag forces, the standard deviation of the excitation forces and the dominant vortex shedding frequency as a function of the relative position of two cylinders restrained from motion. We propose, based on analysis and observations during experiments, that the wake induced oscillation (WIO) behaviour determines if the risers collide or not, and that the vortex-induced vibration (VIV) behaviour determines most of the energy in the collision. That is, the wake behaviour controls the gross motions of the risers relative to each other. The current version is limited to handle two cylindrical risers in staggered and tandem configurations. The results from the simulations are successfully compared with experimental data. TRICE predicts the minimum current when collisions occur with a deviation typically better than 8% for both tandem and staggered arrangements.

1. INTRODUCTION

We have developed a time domain simulator which simulates the dynamic interaction of two adjacent cylindrical risers moving relative to each other in an ambient steady flow. The main objective of the simulator is to assess whether adjacent marine risers moving in each other's wake will collide or not. A secondary goal is to obtain an estimate of the collision velocities between the moving risers, which again is used to do damage and fatigue assessments. This information is subsequently used in the design of riser arrays with respect to riser spacing and to assess the need for vortex-induced vibration (VIV) suppression devices.

A more accurate tool for assessing riser collision has become increasingly more important when oil and gas exploration offshore moves to deeper water, since the risk of collision between marine risers increases with the riser length. In fact, the riser deflection increases with the square of the riser length for a tensioned riser. Collisions may be damaging to the risers from a fatigue point of view, and also by a single collision event if the collision takes

0889–9746/02/030375 + 16 $35.00/0

place with a sufficiently high impact energy. The risers are exposed to current (varying with depth) over a very long length relative to the diameter, and the flow around the risers will cause large interaction effects, see for instance Figure 5 and Zdravkovich (1987) where the drag and lift coefficients are plotted versus relative riser positions. This WIO will cause an irregular riser motion occurring at the first natural mode of motion. The WIO motion is at a frequency substantially lower than the vortex shedding frequency, causing VIV in a higher mode of motion.

1.1. Functionality

Input data to the simulator, named TRICE (Time domain RIser Collision Evaluation), are riser configuration (spacing) and the magnitude and direction of the ambient steady current. Output consists of (i) an accurate estimate of the minimum ambient current velocity which will result in the first collision, and (ii) an estimate of collision frequency and velocities. The estimate of the collision velocity is used together with an estimate of the riser's participating collision mass to obtain an estimate of the impact energy, which is required for fatigue and wear and tear analysis. Trice uses drag and lift coefficients computed by an in-house developed numerical Navier–Stokes equation solver (Herfjord 1996). The computational fluid dynamics (CFD) program computes the amplitudes of the mean and oscillating lift and drag coefficients for both cylinders as well as the nondimensional excitation frequency, hereafter referred to as the Strouhal frequency, as a function of the relative position of two cylinders restrained from moving. The subsequent use of the coefficients in the dynamic analysis is based on a quasistatic approach since the cylinders are restrained form moving during the calculations.

The riser excitation loads are calculated using strip theory, based on the mean and the oscillating drag and lift forces as a function of the relative riser positions. The gross motion of the riser, denoted WIO (wake-induced oscillation) is controlled by the level of the ambient current and the mean lift and drag coefficients. Notice that the mean coefficients are time-varying since the relative riser positions are time-varying.

Based on observations from experiments and simulations, we postulate that the WIO behaviour determines whether the risers collide or not. The VIV motion governs the impact velocity, hence the impact energy. The quasistatic assumption made in the CFD calculations is justifiable, since the vortex shedding frequency is normally much higher than the riser's first eigenfrequency. Hence, the proposed solution is valid if the gross motion behaviour of the riser occurs at frequencies below the first lock-in regime. The current version is limited to handle two risers in staggered and tandem configuration. The observed increase in drag due to VIV (Griffin 1992) is not modelled. However, the transverse forces, and consequently the resulting increase in drag, become small when the risers are in close proximity. Thus, the proposed method is valid to obtain the required riser collision data within the required engineering accuracy.

Comparisons with full-scale experimental data from a towing tank are included in the text.

2. VALIDATION OF THE CODE AND THE RELEVANCE OF THE APPROACH

We assume that a 2-D strip model for the hydrodynamic excitation forces of the riser array is valid and that conventional strip theory is valid for the load functions on 3-D risers. An underlying assumption is that the relevant physical phenomena are described with reasonable accuracy by doing the CFD simulations at a Reynolds number of 200. The full-scale Reynolds number is in the order of 10^5, thus there are some differences in flow details that

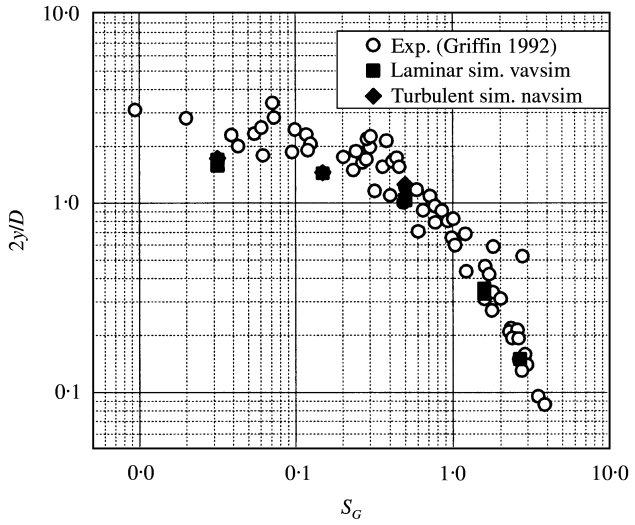

Figure 1. Comparisons of experimental results compiled by Griffin (1992) and the Navsim CFD code.

should be mentioned. At Re = 200, the boundary layer is laminar, while at Re = 10^5, there is a transition to turbulence in the boundary layer. Even if the wake has become unstable and turbulent at Re = 200, the vortical structures are different from those at higher Reynolds number. The smaller vortical structures at Re = 10^5 result in a shorter correlation length compared to the lower Reynolds number. Even so, the amplitude of the lift force does not necessarily decrease with increasing Reynolds number. This may be observed in a figure reported in Pantazopoulos (1994). One further indication of the relevance of the approach is the fact that the correlation length increases considerably as the cylinder starts to move. This is observed through validation work and comparison with measurements reported below.

The CFD code used (named Navsim) has been validated through comparison with a large number of published experiments and numerical results. This is reported in Herfjord (1996). Further development of the code is reported in Herfjord (1999) and Herfjord *et al.* (1999). The classic validation case is the fixed circular section, where the computed drag coefficients are compared with results from experimentally obtained data as a function of Reynolds number. This is reported in the above-mentioned references. Figure 1 contains a comparison with experimental results compiled by Griffin (1992) and results produced by the Navsim CFD code running with Reynolds number at 200 and 40 000. Figure 1 plots the double-amplitude of the response as a function of the reduced damping parameter S_G; $S_G = 8\pi^2 \mathrm{St}^2 \zeta m/\rho D^2$, where $\mathrm{St} = f_S D/U$ is the Strouhal number, ζ is the material damping ratio, U is ambient current velocity, D is riser diameter, ρ is water density and m is the mass per unit length of the cylinder. The results in Griffin (1992) refer to experiments carried out with Reynolds numbers ranging from 300 to 10^6. The results from the simulations are consistent and show reasonable accuracy compared to the measurements reported in a later section. In the present article, a low Reynolds number is used in the CFD runs for obtaining data for a large number of relative positions between the risers. The computations in the applied flow regime are robust and relatively fast. Both physical and numerical experiments have shown that the main vortical structures deciding the interaction effects are adequately modelled. This is shown by Kamemoto (1976), for example, who did experiments with two cylinders in a side-by-side configuration. The Reynolds numbers were 662 and 30 000,

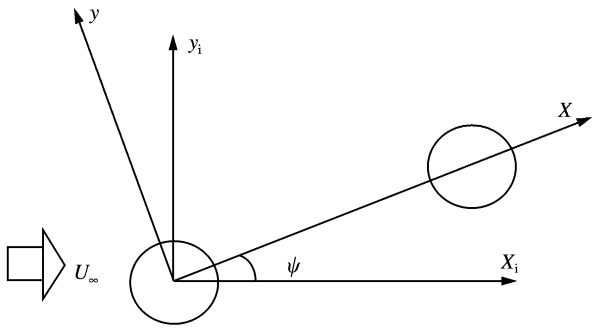

Figure 2. The inertial reference frame (subscript i) and the cylinder-fixed frame of reference shown with a relative inflow angle of ψ.

yielding the same frequency of vortex shedding. Triantafyllou (1998) also claims, based on both theory and experiments, that the dependence on the Reynolds number of the excitation forces is weak, at least in the subcritical regime.

Notice that we do not claim that the flow is fully modelled in all details by using the smaller Reynolds number. However, the gross behaviour, important for the present purpose, is modelled with an accuracy suitable for the chosen approach and application. In Khalak & Williamson (1999) some differences between low-Reynolds number and high-Reynolds number experiments (and simulations) are treated. A collection of data from different investigators show some difference in the VIV response. In the present application, we use results from computations with fixed cylinders. However, exact results for prototype conditions cannot be expected. Like many investigators presenting new applications based on CFD, see for instance C. Y. Zhou & Lam (1999), the ability to simulate physical processes is first demonstrated by using low-Reynolds number simulations. This is done in a subsequent section, reporting validations against model test results on interfering risers, showing promising results. This indicates that an improvement of the force data base to include high-Reynolds number data would make the methodology fully valid for prototype riser arrays.

3. THE MATHEMATICAL MODEL

In this section, the mathematical model is presented which is used by our simulator to simulate the motion of two risers moving relative to each other in each other's wake field.

3.1. The Kinematics

We will use two reference frames in our study: one inertial and the other cylinder fixed. The constant ambient current, denoted by U_∞, will always be in the inertial fixed x-direction. The relative inflow angle between a line starting at the origin of the cylinder fixed reference frame and passing through the centre of the downstream cylinder, and the x-axis of the inertial reference frame is denoted by ψ (in radians). Hence $\psi = 0$ represents a tandem configuration, $\psi = \pm \pi/2$ represents a side-by side configuration and $\psi \in \langle 0, \pm \pi/2 \rangle$ represents staggered arrangements, see Figure 2.

The velocity vector $\boldsymbol{v} = [u, v]^{\mathrm{T}}$ in a cylinder fixed reference frame, moving relative to an inertial system I, can be transformed to an inertial fixed velocity vector $\dot{\boldsymbol{\eta}} = [\dot{x}, \dot{y}]^{\mathrm{T}}$ by using the coordinate transformation matrix $\mathbf{J}(x, y)$ such as $\dot{\boldsymbol{\eta}} = \mathbf{J}(x, y)\boldsymbol{v}$. The lift and drag forces are only dependent on the relative position between the two cylinders and not their orientation,

hence the force coefficients are invariant to the orientation of the moving cylinder. Thus, the coordinate transformation matrix becomes the identity matrix for the cylinder geometry and $\boldsymbol{v}$ can be written as $\boldsymbol{v} = [\dot{x}, \dot{y}]^{\mathrm{T}}$.

3.2. 3-D Dynamics

This section will model the motion of one riser in a riser array in steady ambient flow in 3 degrees of freedom (3-D). The Euler–Bernoulli beam equation with damping describes the motion of one marine riser in time and space:

$$\ddot{x} + \frac{c_\lambda}{m}\dot{x} + \frac{c_u}{m}\dot{x}_r + \frac{\partial^2}{\partial z^2}\left(\frac{EI}{m}\frac{\partial^2 x}{\partial z^2}\right) - \frac{1}{m}\frac{\partial}{\partial z}\left(T\frac{\partial x}{\partial z}\right) = \frac{1}{m}f(t, \Delta x, \Delta y, z), \tag{1}$$

where x (or y) and z are states representing transverse x (or y) position and the position along the riser, respectively, m denotes the beam mass per unit length including the added mass, c_λ and c_u are the linear damping parameters due to structural dissipation and dissipation of energy due to the relative velocity $\dot{x}_r$ between the riser and the ambient water, EI is the riser stiffness, T is axial tension and $f(t, z)$ represents excitation (hydrodynamic) forces in the x (or y) direction, such as lift and drag forces. The terms Δx and Δy represent the relative riser spacing (gap) between the risers in the x- and y-direction. We use the term added mass throughout this article even though acceleration-dependent forces is a better and more accurate term for this physical effect. The eigenfrequencies of this system are analytically found to be

$$\omega_n = \frac{\pi n}{L}\sqrt{\frac{T}{m}}\left(1 + \frac{EI}{T}\frac{\pi^2}{L^2}n^2\right)^{\frac{1}{2}}, \quad n = 1, \ldots, \infty. \tag{2}$$

Equation (1) can be simulated in time and space by representing the fourth-order partial differential equation in equation (1) with a finite element model. The real challenge with the model in equation (1) is to determine the external force function $f(t, z)$. The combined wake field from all the risers in the riser array will determine this function. This wake will be a function of the relative riser positions and velocities, the magnitude and direction of the ambient current and the physical riser properties (dimensions, weight and stiffness). This function is discussed in more detail in a later section.

3.3. 2-D Dynamics

The fourth-order partial differential equations in equation (1) can, for a 2-D case, be simplified by using strip theory to the following set of second-order differential equations:

$$\begin{aligned} \ddot{x} + 2\lambda\bar{\omega}_n\dot{x} + \bar{\omega}_n^2 x &= \mu f_D(\Delta x, \Delta y, t), \\ \ddot{y} + 2\lambda\bar{\omega}_n\dot{y} + \bar{\omega}_n^2 y &= \mu f_L(\Delta x, \Delta y, t), \end{aligned} \tag{3}$$

where λ is the relative damping ratio, in which the effect of both material damping and the damping effect due to relative motion between the strip and ambient water particles are lumped, $\bar{\omega}_n$ represents the two-dimensional system natural frequency found from $\bar{\omega}_n = \sqrt{k/m}$, k is the riser-strip restoring force from the riser's rigidity (combined effect of stiffness EI and tension T) for this particular z-coordinate along the riser, μ is the strip mass ratio $\mu = 1/m$, and the nonlinear excitation forces $f_D(\Delta x, \Delta y, t)$ and $f_L(\Delta x, \Delta y, t)$ represent the external forces from in-line drag force and transverse lift force, respectively. The functions

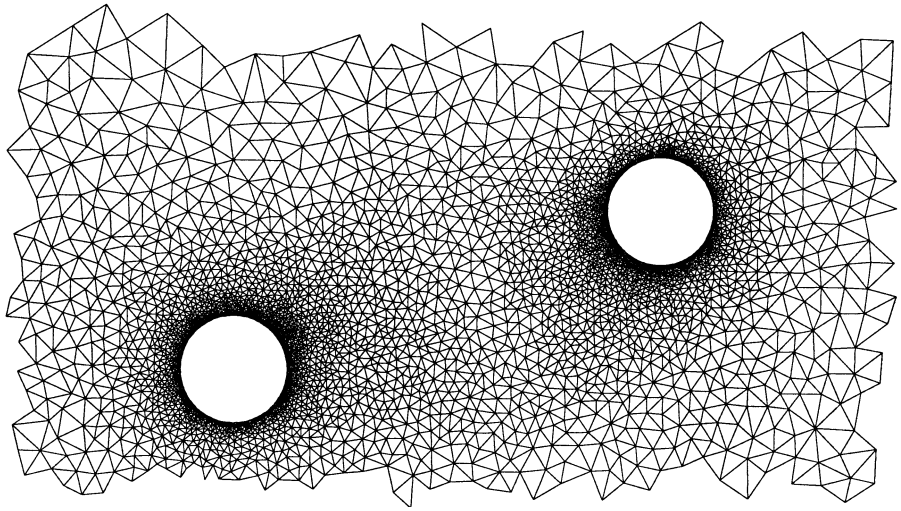

Figure 3. An example of a grid used in the CFD computations.

$f_D(\Delta x, \Delta y, t)$ and $f_L(\Delta x, \Delta y, t)$ are highly nonlinear and vary strongly with respect to Δx and Δy.

The 2-D natural frequency $\bar{\omega}_n$ is found by using the 2-D mass and the stiffness k of the riser at the particular position along the riser from a second-order linear analytical solution to the static problem of a beam in tension (1).

The restoring forces from the riser's rigidity are induced by moving the riser away from its equilibrium. For the 2-degree-of-freedom case this force can locally be modelled for each strip as a restoring spring force f_s which is linear in the riser displacement x as follows:

$$f_s = k(z)(x_d - x_o), \tag{4}$$

where $k(z)$ represents the equivalent stiffness per unit length as a function of z, x_d is the displacement vector from the equilibrium position x_o when no external forces are present. The 3-D FEM-based version calculates the restoring force directly as a part of its stiffness matrix.

The dissipative linear damping ratio λ is assumed constant and always set to 0.3. This is based on observations of the gross motion behaviour of the model scale risers during installation and testing prior to the experiments.

4. THE HYDRODYNAMIC EXCITATION FORCES

The drag and lift force functions $f_D(\Delta x, \Delta y, t)$ and $f_L(\Delta x, \Delta y, t)$ are determined from a large set of CFD computations calculating the lift and drag coefficients. The standard deviations and peak frequencies of the forces in both directions are computed for both cylinders as a function of the relative riser position. The driving forces in equation (5) below are based on the definition of excitation forces used by the numerical Navier–Stokes solver:

$$f_{D/L}(\Delta x, \Delta y, t) = \tfrac{1}{2}\rho C_{D/L}(\Delta x, \Delta y, t)\, D\, |U_\infty| U_\infty, \tag{5}$$

where ρ is the density of the ambient fluid, and U_∞ the magnitude of the ambient current. The lift and drag coefficients as well as the local Strouhal numbers are found for both cylinders by running the CFD program on a 2-D model of two risers restrained from moving in steady flow. The CFD program is thoroughly described in Herfjord (1996) and Herfjord & Faltinsen (1994). A typical model used by the CFD program is shown in Figure 3. Figure 4 illustrates the positions where the calculations have been made. We have

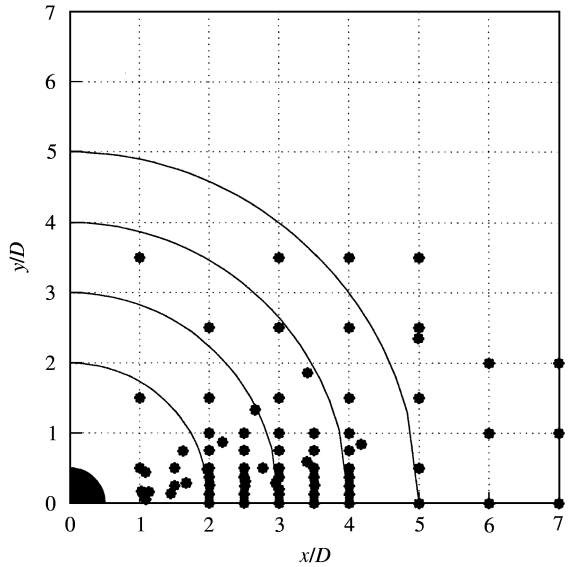

Figure 4. Points used in the CFD computations. An additional 16 points are used with x/D values up to 40 (x/D).

used cubic splines to generate a regular mesh with knots on each $\frac{D}{5}$. Some points at relative riser spacing of 10, 20 and 30D were also calculated, to check for sensitivity and to obtain proper boundary conditions for the interpolation with cubic splines. The nearest knot is selected during the dynamic simulations. The plots in Figures 5–7 contain nondimensional data for the cylinders, i.e., mean drag and lift, the Strouhal frequency and the standard deviation of the forces for the upstream and downstream cylinders. The lift and drag coefficient are decomposed into two components, one mean and the other oscillating as follows:

$$C_{L/D}^{\text{Total}}(\Delta x, \Delta y, t) = C_{L/D}^{\text{mean}}(\Delta x, \Delta y) + C_{L/D}^{\text{osc}}(\Delta x, \Delta y), \tag{6}$$

where $C_{L/D}^{\text{osc}}(x, y)$ can, for a narrow peaked (little damping) spectrum be modelled as follows:

$$C_{L/D}^{\text{osc}}(\Delta x, \Delta y) = \sqrt{2\text{Std}(C_{L/D}(\Delta x, \Delta y))}\sin\left(\frac{2\pi\text{St}(\Delta x, \Delta y)U_\infty}{D}t\right), \tag{7}$$

where the term $\text{Std}(C_{L/D}(\Delta x, \Delta y))$ represents the standard deviation of the force and $\text{St}(\Delta x, \Delta y)$ is the Strouhal frequency for the same force. The following approach is more suitable in a stochastic realization of the simulator:

$$C_{L/D}^{\text{osc}}(\Delta x, \Delta y) = \frac{e_k s}{s^2 + 2\lambda_{HF}\omega s + \omega^2}, \tag{8}$$

where $\omega = 2\pi\text{St}(x, y)U_\infty/D$, λ_{HF} is the spectrum damping ratio. The spectrum peaks are very narrow, thus λ_{HF} is set to a constant 0·05; e_k is the white-noise input with covariance tuned according to $\text{Var}(C_{L/D}(x, y))$. The CFD calculations sometimes resulted in a two peaked spectrum of the oscillatory forces. We always selected the peak with the most energy and neglected the other peaks in our calculations.

4.1. The Effect of VIV on the Drag Coefficient

Single cylinders free to move in an ambient flow will experience an increased drag according to the transverse motion. The drag force may be increased by as much as a factor of 3 (Griffin 1992). In case of two or more cylinders, the presence of a downstream cylinder will have little influence on the behaviour of an upstream cylinder if the distance between upstream and downstream cylinders is more than $5D$. However, in the area roughly confined by the rectangle 3 to $5D$ in-line and 2 to $3D$ transverse to the flow, the cylinder in the wake affects the flow around the upstream cylinder in such a way that the transverse dynamic force is decreased significantly. Thus, as the two cylinders approach each other, the transverse dynamic excitation on the upstream cylinder approaches zero. This observation is based on the quasistatic computations. However, computations with dynamic cylinders (with the cylinders moving relative to each other) have been performed for positions ($x/D = 4$, $y/D = 0$) and ($x/D = 4$, $y/D = 1{\cdot}5$), (Herfjord 1999). For moderate transverse motion, that is with response amplitudes ($y/D < 0{\cdot}2$) the mean drag for a cylinder free to move is less than 10% larger than for a fixed one.

4.2. Comparison with Data in the Literature

The drag coefficients for the downstream cylinder in the bottom-left plot in Figure 5 are very similar to the model test data reported in Zdravkovich (1987). The main difference between the CFD results and those presented in Zdravkovich (1987) is that our C_D is somewhat higher for $y/D > 1$. The mean transverse force on the downstream cylinder as a function of relative position to the upstream cylinder is shown in the bottom-right plot of Figure 5. The trends and the spatial changes of the lift coefficients are also similar to Zdravkovich's (1987), but our values are smaller, i.e., the absolute value is smaller. The nondimensional frequencies shown in the top- and bottom-right plots of Figure 6 compare well with the corresponding experimentally obtained data in Zdravkovich (1987). We have not been able to find any references to Strouhal numbers for the longitudinal force component of either the upstream or the downstream cylinder. Comparing the results with those in Okajima (1979) for tandem arrangements of riser, we notice that we have a good match with respect to C_D values along the $y = 0$ line for both the downstream and the upstream cylinder, see Figures 5 and 6. Our peak frequencies are higher Okajima's (1979) both for the upstream and downstream cylinders and especially for large y/D values.

Figure 7 gives the standard deviations of the variations in the computed force coefficients.

5. COMPARISON BETWEEN TRICE AND THE EXPERIMENTAL DATA

5.1. The Experimental Set-up

A model scale experiment has been carried out in Marintek's towing tank no. 3 which is 10·5 m wide and 10 m deep; 50 m of the total tank length of 85 m was used in the experiment. The experiment was originally performed in a VIV study as part of the Norwegian Deepwater Program sponsored by numerous oil companies operating in the North Sea. However, data from the experiments were made available for other purposes too. Five 10 m 1 : 100 models of a 1000 m riser array were mounted vertically on a truss structure which was towed in the tank, see Figure 8. The risers were pre-tensioned by springs and fixed by universal joints on the bottom. The risers were mounted with hinged–hinged boundary conditions and free to rotate around the length axis at the top, but restrained from rotating at the bottom. The truss structure was prevented from vibrating by

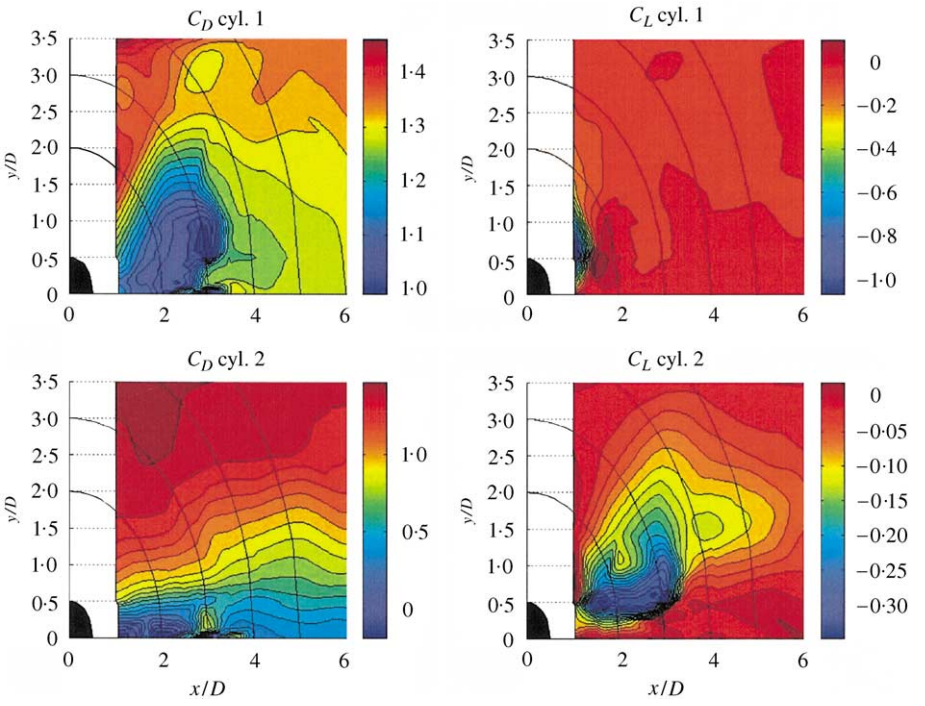

Figure 5. Mean force coefficients. Top left: the drag coefficient of the upstream cylinder. Top right: the lift coefficient of the upstream cylinder. Bottom left: the drag coefficient of the downstream cylinder. Bottom right: the lift coefficient of the downstream cylinder. All coefficients are nondimensionalized according to equation (5). The data are plotted as functions of nondimensional relative cylinder positions; the positions are made dimensionless with respect to riser diameter D.

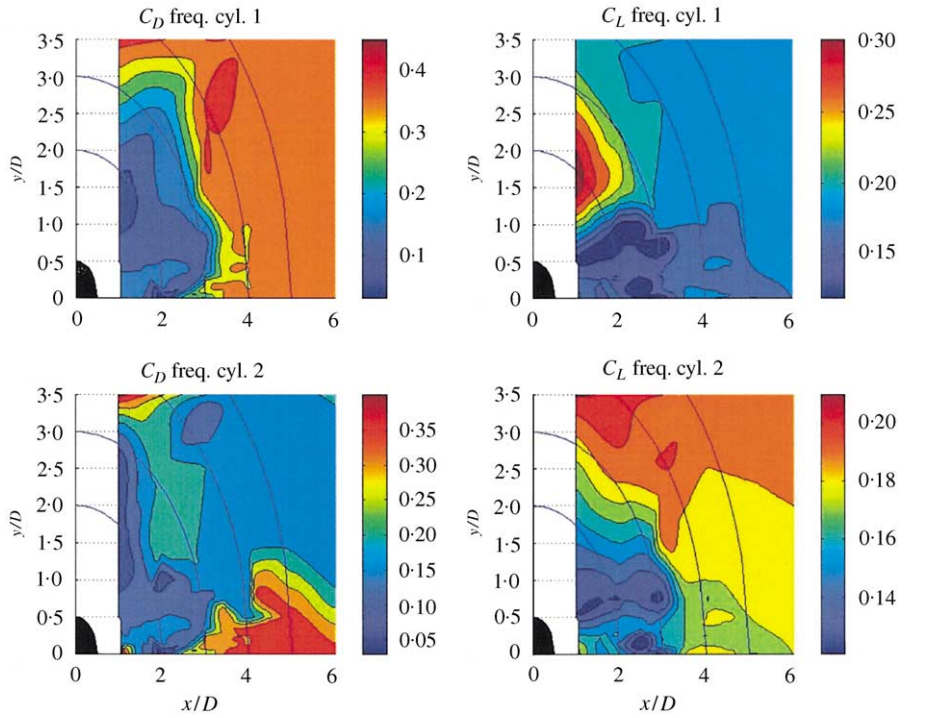

Figure 6. The nondimensional frequency of the force variation (Strouhal frequency). Top left: the Strouhal frequency for the drag forces for the upstream cylinder. Top right: the Strouhal frequency for the lift forces for the upstream cylinder. Bottom left: the Strouhal frequency for the drag forces for the downstream cylinder. Bottom right: the Strouhal frequency for the lift forces for the downstream cylinder. The data are plotted as functions of nondimensional relative cylinder positions, made dimensionless with respect to D.

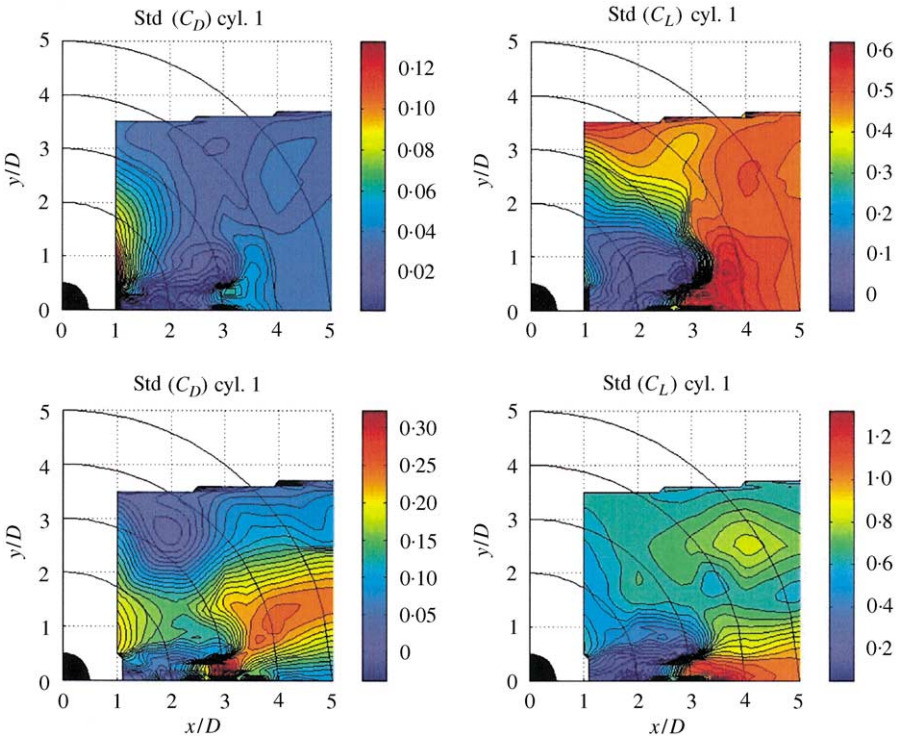

Figure 7. The standard deviations of the variation of the force coefficients. Top left: the standard deviation of the drag forces for the upstream cylinder. Top right: for the lift forces on the upstream cylinder. Bottom left: for the drag forces on the downstream cylinder. Bottom right: for the lift forces on the downstream cylinder. The data are plotted as functions of nondimensional relative cylinder positions, made dimensionless with respect to D.

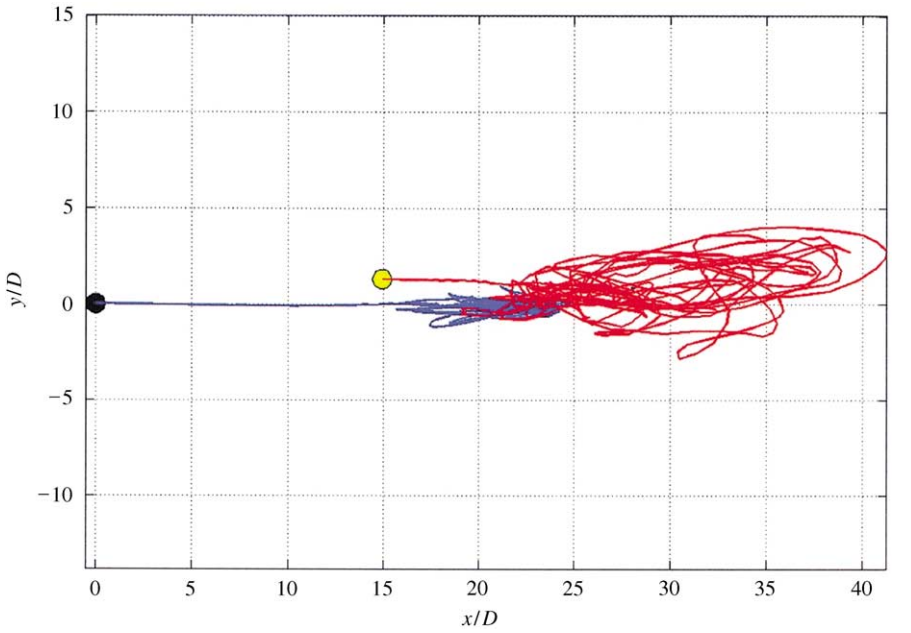

Figure 12. An x–y plot showing the trace of the simulated positions of the two cylinders with the simulator input given in Section 5.2. The positions are made dimensionless with respect to the cylinder diameter, D.

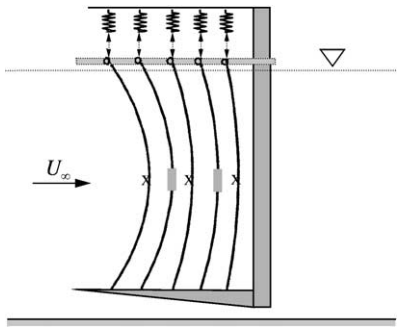

Figure 8. The experimental set-up. Instrumentation: ×, accelerometer (internal, in-line and transverse VIV); ▮, collision impulse; ○, horizontal drag force; ↕ top tension; *, accelerometer (external, transverse VIV).

using guy lines. The whole set-up was towed along the tank, producing an undisturbed in-flow velocity.

The riser models consisted of stainless-steel pipes with outer diameter of 0·010 m and 1·0 mm wall-thickness. The length of each pipe was 10·00 m, of which 9·66 m was submerged in water. The centre to centre spacing between the two risers was always 15 D. The following angles between a line passing through the centre of all the risers and the current direction were tested: 0, 2·5, 5 and 10°. The risers were filled with water during the tests. The risers were pre-tensioned to a nominal tension of 100 N by using a spring arrangement. The actual tension for each riser model was recorded during the tests. Two accelerometers were located at the mid point of the two foremost risers measuring acceleration in the x- and y-direction. A force sensor was also mounted on the mid-point of the risers, measuring contact forces in collision. This sensor was specially designed for this experiment by Marintek. The band-width of the force sensor was measured to be in the area of 600 Hz in water, and the resolution was found to be in the range of $\pm 0{\cdot}1$ N. The force and accelerometers were sampled at 6 kHz after low-pass filtering at 2 kHz. The accelerometer was selected to measure the collision events; thus, the relatively low-frequency WIO-induced accelerations are not measured by the accelerometers. The experiment and resulting data are described in detail in the NDP report (Huse, 1998). Numerous other force transducers and accelerometers were also used during the experiment. The risers were also videotaped with two cameras during the experiments: one camera with a frontal view and the other with a sideways view to the model.

5.2. The Model Scale

The riser model was meant to be a general pre-tensioned riser model on 1 : 100 scale. Most model tests of offshore structures include waves. In such cases, all quantities have to be scaled according to Froude's law of scaling. In the present case, where waves were not involved, we were free to deviate from Froude scaling. For instance, one possibility is to apply equal velocity scaling (EVS) which means that the tests are done at a model velocity which is equal to the velocities experienced in full scale. Denoting the scale factor by γ (linear length), the scaling factor for some of the most important physical parameters are presented in Table 1. EVS was used in the experiment. The main reason was to have correct modelling of the bending stiffness of the risers, which was necessary in order to get correct VIV response and thus collision phenomena. The key issue here is that the modulus of elasticity becomes equal in both the scale model and the full scale riser; that is, the nondimensional bending stiffness parameter $K_{BS} = EI/(\rho D^4 U_\infty)$ becomes equal for the two.

TABLE 1
Froude scaling compared to EVS scaling; γ is scale and ρ_p/ρ_m represents the ratio between density of water for the full scale and model. $\rho_p/\rho_m = 1$ and $\gamma = 100$ in the experiment

Parameter	Froude	EVS
Length	γ	γ
Time	$\gamma^{1/2}$	γ
Velocity	$\gamma^{1/2}$	1
Acceleration	1	γ^{-1}
Force	$\gamma^3 \frac{\rho_p}{\rho_m}$	$\gamma^2 \frac{\rho_p}{\rho_m}$
Momentum	$\gamma^{7/2} \frac{\rho_p}{\rho_m}$	$\gamma^3 \frac{\rho_p}{\rho_m}$
Mass	$\gamma^3 \frac{\rho_p}{\rho_m}$	$\gamma^3 \frac{\rho_p}{\rho_m}$
Modulus of elasticity	$\gamma \frac{\rho_p}{\rho_m}$	$\frac{\rho_p}{\rho_m}$

This implies that we can make the scale model in the same material as the full-scale riser, i.e., steel. This reduces the complexity and costs of the experiment substantially. A further advantage of EVS compared to Froude scaling for this experiment is that the Reynolds number becomes larger due to larger velocity. Finally, higher velocities result in higher forces and thus more robust and accurate transducers and measurements.

5.3. WIO AND VIV

Detailed studies of videotapes and numerical data from the experiments described in a later section have revealed the relatively slow gross motion guided by the wake-induced oscillation controls, whether the risers collide or not. On the other hand, the high-frequency (and high-velocity) VIV motion accounts for most of the energy in the collisions between the risers (Sagatun *et al.* 1999). We did not measure the velocity or the position of the risers (except on video), but we can observe the accumulated (over the riser length) effect of the drag and lift force on the riser through the riser's top tension by using equation (1). The bottom plot of Figure 9 shows the dynamic top tension of the two foremost risers in one of the experiments. The ambient current U_∞ was 0·592 m/s, the top tension was 100 N and the relative inflow angle was 2·5°, see Figure 2. The acceleration in the transverse direction and the recorded impulsive force on the second riser are presented in the top and middle plot in the same figure. By correlating these plots with the video tapes we can conclude that the slow WIO-induced motion controls the relative positions of the risers, while the VIV vibrations account for most of the energy in the collisions. The VIV frequency was approximately 59·7 rad/s and the acceleration amplitudes in the collision free periods were approximately $\pm$ 10 m/s^2). This corresponds to a vibration amplitude of $A = 0{\cdot}28\ D$ with $D = 0{\cdot}01$ m (using $A\omega^2 = a_{\text{measured}}$), which is according to the magnitudes observed on the videos. These data result in an equivalent Strouhal number of 0·160, which compares well with the frequency calculated in Figure 6. The peak VIV velocity becomes $A\omega = 16{\cdot}8$ m/s which is at least an order of larger than the WIO-induced motion shown indirectly in the bottom plot in Figure 9. Figure 10 shows a detailed window of one of the collision events for this particular experimental run. Notice that, by comparing the top and the bottom plot in

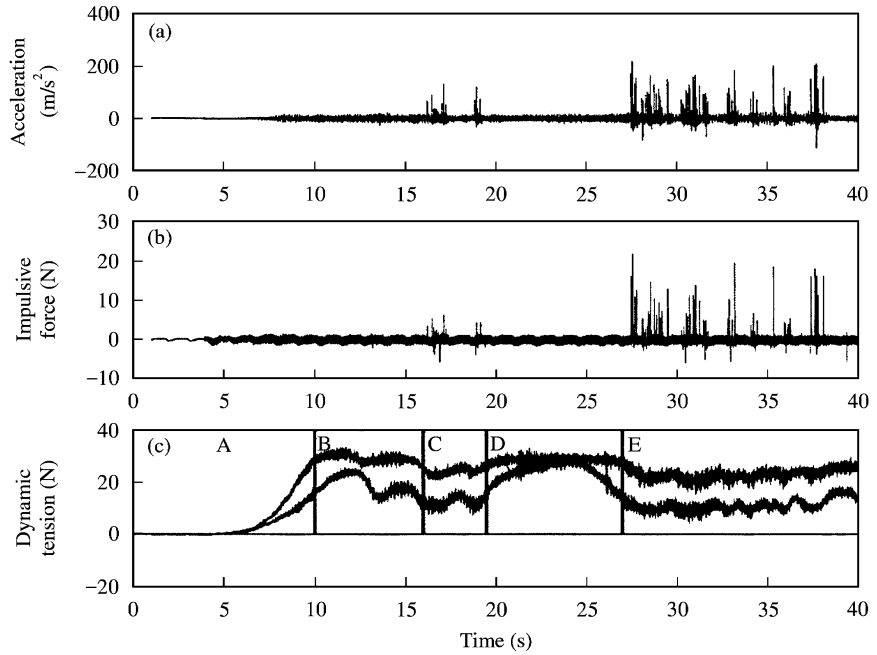

Figure 9. Experimental run 475: $U_\infty = 0{\cdot}592$ m/s, top tension is 100 N and in-flow angle is 2·5°. (a) Acceleration in transverse direction for the mid-point of the second riser. (b) Impulsive force measured in the transverse direction for the second riser. (c) Dynamic top tension (tension − 100 N) of riser 1 (largest tension) and riser 2 (lowest tension). Period A is the time frame when the velocity is ramped up, and no collisions occur. The risers are separated by several *D* in Period B and D. The risers are moving in close proximity to each other and are frequently colliding in period C and E.

Figure 10 we can clearly observe that the top tension vibrates with the double VIV frequency.

5.4. The 3-D Simulation

The 3-D numerical experiment is carried out using a finite-element-based software system. The two risers are modelled using 2 pipes with 10 FE beam elements per pipe. The top tension spring with stiffness 932 N/m is included. Top tension of 100 N as well as the gravity force is applied prior to the hydrodynamic simulation. The speed was varied between 0·4 and 1 m/s and increased in steps of 0·02 m/s. The current is increased linearly from zero to the actual speed over the first 10 s of the dynamic simulation. The simulator was run with different angles of attack. The following angles between a straight line running through the two riser centres and the current direction were run: 0, 2·5, 5 and 10°. The geometrical properties and the boundary conditions were equal to the real-world experiment described in the previous section. The simulator was run in 30 s.

5.5. The 2-D Simulation

The 2-D numerical experiment uses two rigid-body with stripe stiffness and mass. The resulting 2-D stripe stiffness at the mid-point of the beam is calculated to be $k = 7{\cdot}659$ N/m^2. Notice that the geometric stiffness due to a top tension of $T = 100$ N accounts for more than 95% of the total rigidity of the riser. The 2-D strip mass (including added mass) of the water filled steel riser model was set to 0·349 kg/m. The first

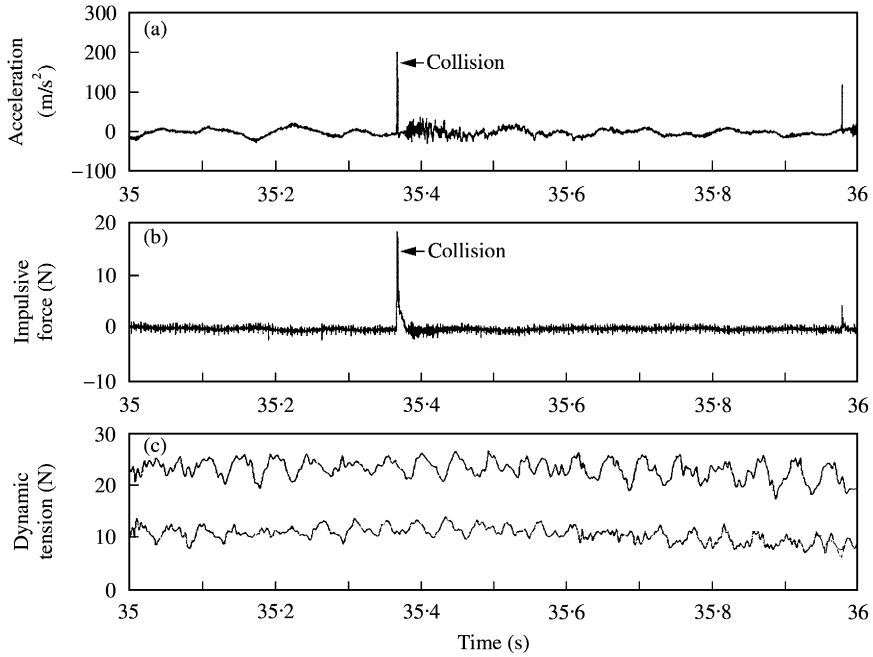

Figure 10. Details from experimental run 475: $U_\infty = 0{\cdot}592$ m/s, top tension is 100 N and in-flow angle is 2·5°. (a) Acceleration in transverse direction for the mid-point of the second riser. (b) Impulsive force measured in the transverse direction for the second riser. (c) Dynamic top tension (tension − 100 N) of riser 1 (largest tension) and riser 2 (lowest tension). Notice that the top tension oscillates with double the VIV frequency shown in the top plot.

eigenfrequency of the model (the nominal ω) becomes 0·75 Hz, while the excitation frequency (assuming a Strouhal number of 0·2) is 9 Hz. The nominal linear damping ratio λ is constant, set to 0·3. The 2-D simulation was run with the same velocities and angles of attack as the 3-D simulation. The velocity was ramped up from 0 m/s to the nominal towing velocity simulating the ambient current. The simulator was run for 30 s. Figure 11 contains the VIV and the WIO components of the lift coefficients for the downstream cylinder based on a time domain simulation using equation (7). The input data to the simulation were equal to the ones described in the previous section.

5.6. Comparison with Experimental Data

Table 2 contains a comparison between the results from the experiments in the towing tank and the two numerical simulations. The minimum towing velocity before the first collision occurs is the benchmark parameter. We have also included a comparison with Ricol (Huse 1993) where appropriate. The results of the comparison reveal that Trice predicts minimum towing velocity before collision occurs, with an error better than $\pm 8\%$. Deviations between the experimental data and the two Trice simulators may be due to the following: (i) Trice registered a collision when the distance between the risers is equal to 0. Some of these situations in the experiment may yield so small an impulse signal that no collision is detected. This is a likely explanation for the underestimation of velocity in Trice 2-D. (ii) The experiment contained five risers, while Trice only operates with two. The three risers behind the second riser will influence the second riser's wake behaviour. (iii) The top tension of the experiment was not exactly 100 N. Hence, the stiffness parameter in the Trice runs was not 100% correct. (iv) Errors in the load coefficients.

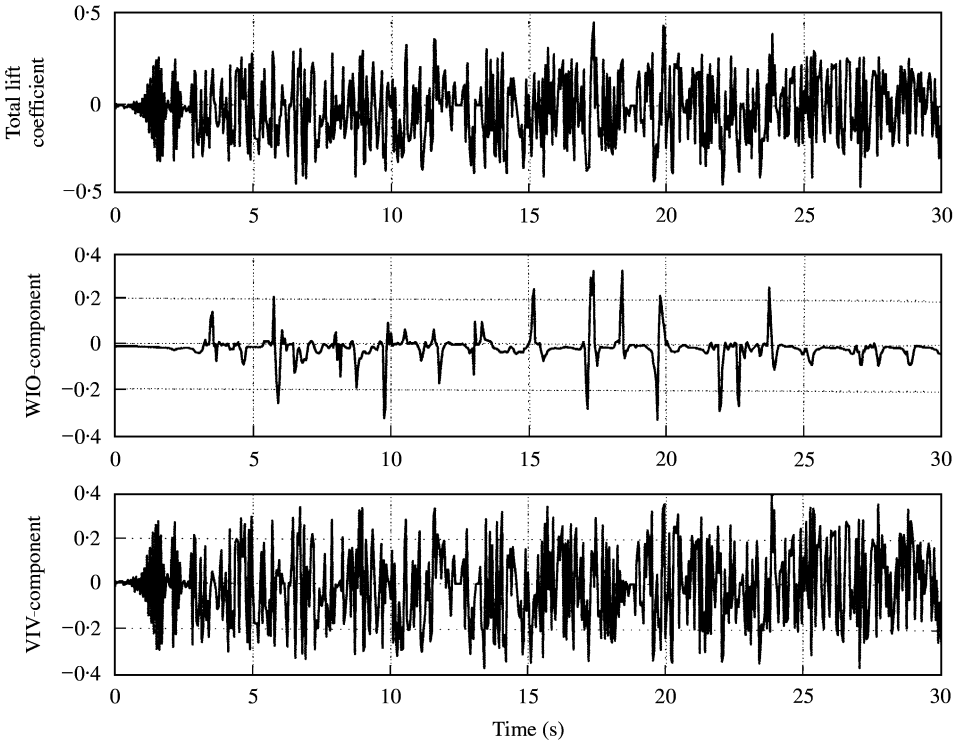

Figure 11. (a) The total lift coefficient for the downstream cylinder plotted as a function of time [s]. (b) The low-frequency (WIO) component of the lift coefficient for the downstream cylinder plotted as a function of time [s]. (c) The high-frequency (VIV) component of the lift coefficient for the downstream cylinder plotted as a function of time [s].

TABLE 2
Comparison between experimental data and numerical models. All numbers in columns 2–5 have units of m/s

Angles deg	Experiment (m/s)	Trice 3-D FEM (m/s)	Trice 2-D Strip (m/s)	Ricol (Huse 1993) (m/s)
0	0·46 – 0·48	0·46	0·44	0·44 – 0·45
2·5	0·43 – 0·48	0·46	0·45	0·5 – 0·6
5	0·48 – 0·53	0·48	0·45	Not valid
10	0·48	0·52	0·47	Not valid

The performance of the Ricol formulation becomes worse when the angle of attack of the current is not zero, since the transverse force is neglected in Ricol. The authors are aware that Ricol has been enhanced to also contain a transverse force based on a correction factor obtained from the experiments described in this article.

6. AN EXAMPLE OF A TRICE SIMULATION

Input data to Trice are riser configuration (spacing and relative angles) and the magnitude and direction of the ambient steady current. The output consists of frequency of collisions

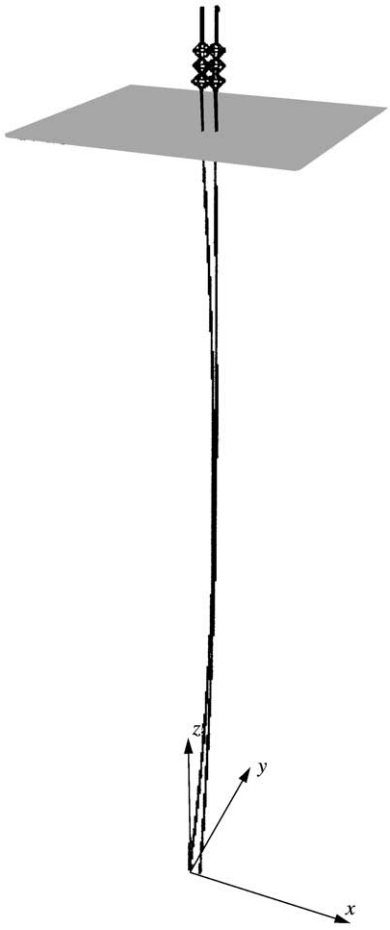

Figure 13. An OpenGl plot of the 3-D simulation of two risers moving in each other's wake.

and collision velocities. Figure 12 †contains a plot of the 2-D simulations of riser positions for a staggered riser configuration in the x–y plane, for a 30 s simulation. The start condition was a staggered arrangement with $\alpha = 5^\circ$ and a $15D$ separation between the two cylinders. The ambient flow U_∞ was gradually increased from 0 to 0·5 m/s; this corresponds to Re $\approx$ 6000. We notice from Figure 12 by looking at the mean y position that the downstream cylinder has been exposed to a net negative lift force. This may be explained by taking into account the lift force coefficient in the bottom-right plot of Figure 5, where we can see that the lift forces will tend to move the downstream cylinder towards the wake centre. We also notice that the drag forces on the downstream cylinder are substantially less than for the first cylinder, hence the risers will move towards each other.

Figure 13 shows an OpenGL plot from the 3-D Trice model of the two risers.

7. CONCLUSION

The purpose of this work has been to create a tool for assessing risk of riser collision as well as statistics on collision velocity. The current version is limited to handle two adjacent

†Figure 12 is found in the colour plate.

cylindrical risers of equal diameter in staggered and tandem configurations. The mean drag, lift, Strouhal numbers and the standard deviation for both drag and lift for both cylinders have been calculated as functions of relative riser positions. These data have been used to generate two nonlinear force functions representing lift and drag forces for the two cylinders moving relative to each other. The resulting performance of the proposed simulators is judged accurately and within the limits required for engineering purposes.

The error margin, for a two-riser system, is less than 10%. This value is valid when checking whether the risers will collide or not. The accuracy of the impact energy assessment, which is also a product of the simulation, is more uncertain. We would also like to stress that we have only compared the simulated results with the experiments described in this article. Further studies and experiments are required to validate this tool for more advanced use.

This proposed simulator has been implemented in two commercially available FEM software products.

ACKNOWLEDGEMENTS

The authors gratefully acknowledge the help and valuable comments from Dr ing. Finn G. Nielsen at Norsk Hydro's research centre in Bergen and Professor Erling Huse at Marintek in Trondheim. The authors would also like to express their gratitude towards the members of the Norwegian Deepwater Program (NDP) and Norsk Hydro Exploration and Production who have permitted that the results from the experiments to be published in this article. Finally, the authors would like to thank the reviewers for numerous comments and helpful remarks.

References

C. Y. Zhou, R. S. & Lam, K. 1999 Vortex-induced vibrations of an elastic circular cylinder. *Journal of Fluids and Structures* **13,** 165–189.

Griffin, O. 1992 Vortex-induced vibrations of marine structures in uniform and sheared flows. *Proceedings of the Workshop on Marine Riser Mechanics*, Ann Arbor, MI, U.S.A.

Herfjord, K. 1996 A Study of two-dimensional separated flow by a combination of the finite element method and Navier–Stokes equation. Ph.D. Thesis, NTH, University of Trondheim, Norway.

Herfjord, K. 1999 Relative body motion. Technical Report Norsk Hydro E and P, FS-Bg 5020 Bergen, Norway. Task report, project ESPRIT 2011 FSI-SD, available on request.

Herfjord, K. & Faltinsen, O. 1994 Viscous effect on slow drift motions. 7*th International Conference on the Behavior of Offshore Structures BOSS*'94, Vol. 2, pp. 147–173.

Herfjord, K., Larsen, C., Furnes, G., Holmås, T. & Randa, K. 1999 FSI simulations of vortex-induced vibrations of offshore structures. *Computational Methods for Fluid Structure Interaction*, pp. 283–303, Trondheim, Norway.

Huse, E. 1993 Interaction in deep-sea riser arrays, *Offshore Technology Conference*, OTC Paper No. 7237.

Huse, E. 1998 Effects of strakes on riser interaction, Technical Report MT51 F98-419/513136.00.02, Marintek, Marintek, Trondheim, Norway. Classification: restricted.

Kamemoto, K. 1976 Formations and interactions of two parallel vortex streets. *Bulletin of the JSME* **19** (129), pp. 283–290.

Khalak, A. & Williamson, C. 1999 Motions, forces and mode transitions in vortex-induced vibrations at low mass-damping, *Journal of Fluids and Structures* **13,** 813–851.

Okajima, A. 1979 Flows around two tandem circular cylinders at very high Reynold's numbers. *Bulletin of the JSME* **22** (166).

Pantazopoulos, M. S. 1994 Vortex-induced vibration parameters: critical review, *OMAE*'94, pp. 199–255.

SAGATUN, S. I., HERFJORD, K., NIELSEN, F. G. & HUSE, E. 1999 Participating mass in colliding risers. *Journal of Marine Science and Technology* **4,** 58–67.

TRIANTAFYLLOU, G. 1998 Vortex induced vibrations of long cylindrical structures. *Proceedings of the* 1998 *ASME Fluids Engineering Division Summer Meeting*, Washington, DC.

ZDRAVKOVICH, M. M. 1987 The effect of interference between circular cylinders in cross flow. *Journal of Fluids and Structures* **1,** 239–261.